Langmuir
Article
pubs.acs.org/Langmuir

DC Electrokinetic Particle Transport in an L-Shaped Microchannel

Ye Ai,[†] Seungkyung Park,[†] Junjie Zhu,[‡] Xiangchun Xuan,[‡] Ali Beskok,[†] and Shizhi Qian*[,†,§]

[†]*Department of Aerospace Engineering, Old Dominion University, Norfolk, Virginia 23529,* [‡]*Department of Mechanical Engineering, Clemson University, Clemson, South Carolina 29634, and* [§]*School of Mechanical Engineering, Yeungnam University Gyongsan 712-749, South Korea*

Received July 23, 2009. Revised Manuscript Received September 11, 2009

Electrokinetic transport of particles through an L-shaped microchannel under DC electric fields is theoretically and experimentally investigated. The emphasis is placed on the direct current (DC) dielectrophoretic (DEP) effect arising from the interactions between the induced spatially nonuniform electric field around the corner and the dielectric particles. A transient multiphysics model is developed in an arbitrary Lagrangian−Eulerian (ALE) framework, which comprises the Navier−Stokes equations for the fluid flow and the Laplace equation for the electrical potential. The predictions of the DEP-induced particle trajectory shift in the L-shaped microchannel are in quantitative agreement with the obtained experimental results. Numerical studies also show that the DEP effect can alter the angular velocity and even the direction of the particle's rotation. Further parametric studies suggest that the L-shaped microfluidic channel may be utilized to focus and separate particles by size via the induced DEP effect.

1. Introduction

The use of electrokinetic means for particle (both biological and synthetic) manipulation, such as separation, assembling, sorting, focusing, and characterization in lab-on-a-chip (LOC) devices, has recently gained significant attention.[1−3] Electrokinetic particle manipulation offers a way to manipulate particles using only electric fields with no moving parts.[4,5] Other inherent advantages include nonintrusion, low cost, easy implementation, and favorable scaling with size.

When spatially uniform DC electric fields are applied to colloidal suspensions confined in a microchannel, particle motion is generally induced by both electrophoretic force acting on the particle and electro-osmotic fluid motion arising from the surface charges at the channel walls. Electrokinetic transport of particles in micro-/nanochannels with simple geometries such as parallel-plate,[6,7] cuboid,[8,9] and cylindrical tube[6,10−13] under uniform electric fields has been extensively studied. It has also been applied to separate and characterized particles on the basis of charges.[14−17]

In the cases of spatially nonuniform electric fields, DC dielectrophoretic (DEP) effect arises along with the above-mentioned electrophoretic and electro-osmotic effects due to the induced dipole moment on the particles. Nonuniform electric fields produce asymmetric net force and torque on the dipoles, yielding the translational and rotational motions of particles. Indeed, most microfluidic channels in LOC devices, for example, L-shaped, Y-shaped, and constricted channels, create nonuniform electric fields, which may induce nontrivial DEP forces on the particles and thus affect the particle transport. Recently, many investigators have utilized the resultant DEP forces under nonuniform DC electric fields in LOC devices for particle manipulation.[5,18−24] For example, Kang et al.[4] experimentally demonstrated the particle trajectory shift in a constricted microchannel due to the DC DEP effect, which was then utilized for particle separation[5,23−27] and focusing.[28,29] Xuan et al.[30] demonstrated that the enhancement of electrokinetic particle transport in a converging-diverging microchannel is much lower than that in a pressure-driven flow because of the DEP retardation effect. Zhu et al.[31] employed the DC DEP force generated in a serpentine microchannel to achieve particle focusing.

Despite of many potential applications of DC DEP manipulations, a comprehensive analysis of electrokinetic particle transport under nonuniform DC electric fields is still limited. The

*Corresponding author. E-mail: sqian@odu.edu.

(1) Hunter, R. J. *Foundations of Colloid Science*, 2nd ed.; Oxford University Press: New York, 2001.
(2) Li, D. Q. *Electrokinetics in Microfluidics*; Elsevier Academic Press: New York, 2004.
(3) Kang, Y. J.; Li, D. Q. *Microfluid. Nanofluid.* **2009**, *6*, 431.
(4) Kang, K. H.; Xuan, X. C.; Kang, Y.; Li, D. *J. Appl. Phys.* **2006**, *99*, 064702.
(5) Kang, Y. J.; Li, D. Q.; Kalams, S. A.; Eid, J. E. *Biomed. Microdevices* **2008**, *10*, 243.
(6) Keh, H. J.; Anderson, J. L. *J. Fluid Mech.* **1985**, *153*, 417.
(7) Unni, H. N.; Keh, H. J.; Yang, C. *Electrophoresis* **2007**, *28*, 658.
(8) Xuan, X. C.; Raghibizadeh, R.; Li, D. *J. Colloid Interface Sci.* **2005**, *296*, 743.
(9) Ye, C. Z.; Li, D. Q. *Microfluid. Nanofluid.* **2004**, *1*, 52.
(10) Qian, S.; Joo, S. W. *Langmuir* **2008**, *24*, 4778.
(11) Qian, S.; Joo, S. W.; Hou, W.; Zhao, X. *Langmuir* **2008**, *24*, 5332.
(12) Xuan, X. C.; Ye, C. Z.; Li, D. Q. *J. Colloid Interface Sci.* **2005**, *289*, 286.
(13) Ye, C. Z.; Xuan, X. C.; Li, D. Q. *Microfluid. Nanofluid.* **2005**, *1*, 234.
(14) Leopold, K.; Dieter, B.; Ernst, K. *Electrophoresis* **2004**, *25*, 2282.
(15) Rodriguez, M. A.; Armstrong, D. W. *J. Chromatogr., B* **2004**, *800*, 7.
(16) Dietrich, K.; Jan, C. T. E.; Albert van den, B.; Richard, B. M. S. *Electrophoresis* **2008**, *29*, 977.
(17) Gloria, O.; Christina, S.; Matthew, B. K.; Anubhav, T.; Anuj, C. *Electrophoresis* **2008**, *29*, 1152.
(18) Cummings, E. B.; Singh, A. K. *Anal. Chem.* **2003**, *75*, 4724.
(19) Blanca, H. L.-E.; Blake, A. S.; Eric, B. C.; Yolanda, F. *Electrophoresis* **2004**, *25*, 1695.
(20) Lapizco-Encinas, B. H.; Simmons, B. A.; Cummings, E. B.; Fintschenko, Y. *Anal. Chem.* **2004**, *76*, 1571.
(21) Ying, L. M.; White, S. S.; Bruckbauer, A.; Meadows, L.; Korchev, Y. E.; Klenerman, D. *Biophys. J.* **2004**, *86*, 1018.
(22) Lapizco-Encinas, B. H.; Rito-Palomares, M. *Electrophoresis* **2007**, *28*, 4521.
(23) Hawkins, B. G.; Smith, A. E.; Syed, Y. A.; Kirby, B. J. *Anal. Chem.* **2007**, *79*, 7291.
(24) Lewpiriyawong, N.; Yang, C.; Lam, Y. C. *Biomicrofluidics* **2008**, *2*, 034105.
(25) Barbulovic-Nad, I.; Xuan, X. C.; Lee, J. S. H.; Li, D. Q. *Lab Chip* **2006**, *6*, 274.
(26) Kang, Y.; Cetin, B.; Wu, Z.; Li, D. *Electrochim. Acta* **2009**, *54*, 1715.
(27) Kang, K. H.; Kang, Y. J.; Xuan, X. C.; Li, D. Q. *Electrophoresis* **2006**, *27*, 694.
(28) Thwar, P. K.; Linderman, J. J.; Burns, M. A. *Electrophoresis* **2007**, *28*, 4572.
(29) Zhu, J.; Xuan, X. *Electrophoresis* **2009**, *30*, 2668.
(30) Xuan, X. C.; Xu, B.; Li, D. Q. *Anal. Chem.* **2005**, *77*, 4323.
(31) Zhu, J.; Tzeng, T.-R.; Hu, G.; Xuan, X. *Microfluid. Nanofluid.* Published online, **2009**, DOI: 10.1007/s10404-009-0432-7.

majority of previous numerical studies of particle electrokinetic transport in nonuniform microchannels, such as L-shaped,[32] T-shaped,[33] converging−diverging nanopores,[34] and nanopore/microchannel junctions,[35] have neglected the DC DEP effect. Young and Li[36] suggested the DEP effect on the electrokinetic particle transport in a microchannel with a uniform cross-section should be taken into account when the distance between the particle and channel wall is comparable to the particle size. In a previous numerical study, we reported that the particle trajectory in a converging-diverging microchannel with considering the DEP effect is in good agreement with the existing experimental data, which, however, significantly deviates from the prediction when the DEP effect is ignored.[37]

In this paper, we present a numerical and experimental investigation of the transient electrokinetic particle transport in an L-shaped microchannel with a full consideration of the particle−fluid−electric field interactions. L-shaped microchannels, the basic unit of U-shaped and T-shaped microchannels, are commonly used to switch the transport direction of fluids and particles in LOC devices.[38] To obtain a precise prediction of particle motion under the induced nonuniform DC electric field, flow and electric fields are solved in a coupled manner. The DEP force exerting on the moving particle is obtained by integrating directly the Maxwell stress tensor over the particle surface, which is regarded as the most rigorous method for the DEP calculation.[39] The structure of the rest of this paper is listed as follows. Section 2 describes the procedure of device fabrication and experimental setup. Section 3 introduces the mathematical model composed of the Navier−Stokes equations for the flow field and the Laplace equation for electric field defined in an arbitrary Lagrangian−Eulerian (ALE) framework. The experimental and numerical results are discussed in section 4 with focuses on the DC DEP effect on particle translation and rotation. Concluding remarks are given in the final section.

2. Experimental Setup

Polystyrene particles of 4 and 10 μm in diameter were purchased from Molecular Probes Inc. (Eugene, OR). As the original particle solution is highly concentrated, further dilution with 1 mM potassium chloride (KCl) solution is necessary to achieve the tracking of a single particle transport. The L-shaped channel, as shown in Figure 1a, was fabricated using a standard soft lithography technique[40] with poly(dimethylsiloxane) (PDMS). Briefly, SU-8 photoresist (Formulation 25, MicroChem Corp., Newton, MA) was first spin-coated on a clean glass slide, followed by a two-step soft bake (65 °C for 3 min and 95 °C for 7 min). Next, the photoresist film was exposed to ultraviolet light under a 3500 dpi mask with a desired L-shaped geometry, followed by another two-step hard bake (65 °C for 1 min and 95 °C for 3 min). After the hard bake, a positive master was obtained by developing the photoresist for 4 min with commercial SU-8 developer solution. Subsequently, the PDMS mixture (Sylgard184 Silicone Elastomer Kit, Dow Corning Corp., Freeland, MI) of prepolymer and curing agent with a ratio of 10:1 by weight were poured over the master and polymerized in a vacuum at 65 °C for 4 h. The cured PDMS with an L-shaped microchannel was then peeled from the master and two holes of 5 mm in diameter were punched to serve as reservoirs. Finally, a two-minute oxygen plasma treatment (Harrick Plasma Inc., Ithaca, NY) was performed to obtain a permanent glass/PDMS bonding and form the desired microchannel. Immediately after the bonding step, the diluted particle solution was driven into the microchannel by capillary force. As illustrated in Figure 1a, the microchannel was measured to be 53 (±1) μm in width and 25 (±1) μm in depth. The length of the entire channel between the two reservoirs was 15 mm.

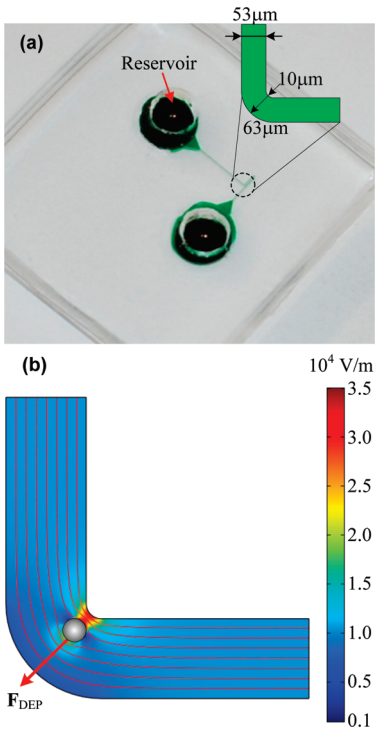

Figure 1. (a) Photograph of an L-shaped PDMS-based microchannel. The channel was filled with green food dye for a clear demonstration. The inset is a schematic view of the channel with actual dimensions. The width of the channel is 53 μm, and the radii of the arc connections at the inner and outer corners are, respectively, 10 and 63 μm. (b) Distribution and streamlines of electric field (10 KV/m in average) within the L-shaped channel in the presence of a particle. The arrow denotes the direction of the DC DEP force exerting on the particle.

The DC electrokinetic particle transport was observed by a CCD camera (PowerviewTM, TSI Inc., Shoreview, MN) equipped in an inverted optical microscope (Nikon Eclipse TE2000U, Nikon Instruments, Lewisville, TX). Pressure-driven flows were carefully eliminated before each experiment by balancing the solution heights in the two reservoirs until particles inside the channel become stationary. Two platinum electrodes of 1 mm in diameter connected to a DC power supply (Circuit Specialists Inc., Mesa, AZ) were placed in the two reservoirs to generate the electrokinetic particle transport. The particle motion was captured at a rate of 7.25 Hz with an exposure time of 100 μs. The captured images with a resolution of 1376 × 1040 pixels were processed using a image processing software ImageJ (National Institutes of Health, http://rsbweb.nih.gov/ij/), to extract the location of the particle's center at each time step. The reading error of the particle's center was about ±2 pixels, corresponding to ±0.645 μm. Particle velocity was calculated by dividing the travel distance of particles over the time step in a series of successive images. Using this method, the relative error of the particle velocity is less than ±4.8%. Finally, the electrokinetic mobility of particles can be estimated by dividing the particle's velocity over the corresponding electric field applied.

(32) Davison, S. M.; Sharp, K. V. *Microfluid. Nanofluid.* **2008**, *4*, 409.
(33) Ye, C. Z.; Li, D. Q. *J. Colloid Interface Sci.* **2004**, *272*, 480.
(34) Qian, S.; Wang, A. H.; Afonien, J. K. *J. Colloid Interface Sci.* **2006**, *303*, 579.
(35) Liu, H.; Qian, S. Z.; Bau, H. H. *Biophys. J.* **2007**, *92*, 1164.
(36) Young, E. W. K.; Li, D. Q. *Langmuir* **2005**, *21*, 12037.
(37) Ai, Y.; Joo, S. W.; Jiang, Y.; Xuan, X.; Qian, S. *Electrophoresis* **2009**, *30*, 2499.
(38) Rhee, M.; Burns, M. A. *Lab Chip* **2008**, *8*, 1365.
(39) Wang, X. J.; Wang, X. B.; Gascoyne, P. R. C. *J. Electrostat.* **1997**, *39*, 277.
(40) Duffy, D. C.; McDonald, J. C.; Schueller, O. J. A.; Whitesides, G. M. *Anal. Chem.* **1998**, *70*, 4974.

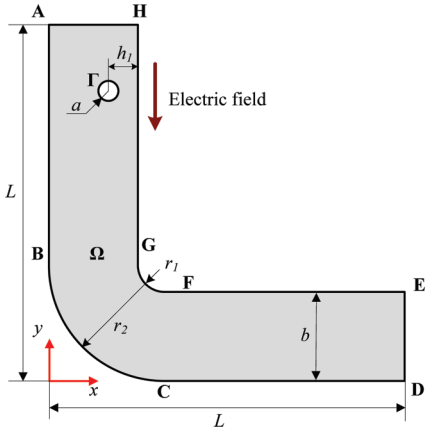

Figure 2. A two-dimensional schematic view of a circular particle of radius a migrating in an L-shaped microchannel. An external electric field, **E**, is applied between the inlet and outlet of the channel.

3. Mathematical Model and Numerical Implementation

A remarkable good agreement between the numerical predictions of electrokinetic particle transport in converging-diverging microfluidic channels, obtained from a two-dimensional (2D) mathematical model, and the experimental data suggests that a 2D model is sufficient to capture the essential physics of the electrokinetic particle transport process.[37] Therefore, a 2D mathematical model is adopted in this study. We consider a circular particle of radius a initially located at the upstream of the L-shaped microchannel with outer length L and width b, as shown in Figure 2. The distance between the particle's center and the inner channel wall is h_1. A two-dimensional Cartesian coordinate system (x, y) with the origin located at the outer corner of the microchannel is used in the present study. The computational domain Ω, surrounded by the channel boundary ABCDEFGH and the particle surface Γ, is filled with 1 mM KCl aqueous solution. Sections ABGH, BCFG, and CDEF in the computational domain Ω are, respectively, defined as the upstream, corner, and downstream of the L-shaped microchannel. The radii of the arc connections at the inner and outer corner are, respectively, r_1 and r_2. The segments AH and DE are, respectively, the inlet and outlet between which an electric potential difference is externally applied. The particle and channel wall are assumed to be rigid and nonconducting. The fluid in the computational domain Ω is incompressible and Newtonian. The effect of Brownian motion can be ignored for micrometer-sized particles.[32] As the thickness of electrical double layer (EDL) is on the order of several nanometers, the thin EDL approximation is valid for microscale electrokinetics concerned in the present study. Hence, the net charge density in the computational domain Ω is zero and the electric potential, ϕ, satisfies the Laplace equation

$$\nabla^2\phi = 0 \qquad \text{in } \Omega \tag{1}$$

All rigid surfaces are electrically insulating,

$$\mathbf{n}\cdot\nabla\phi = 0 \qquad \text{on ABCD, EFGH, and } \Gamma \tag{2}$$

and a potential difference ϕ_0 between the inlet and the outlet is imposed by

$$\phi = \phi_0 \qquad \text{on AH} \tag{3}$$

and

$$\phi = 0 \qquad \text{on DE} \tag{4}$$

In the framework of the thin EDL approximation, the particle and its adjacent EDL are regarded as a single entity. Since the Reynolds number of electrokinetic flows in most LOC applications is usually very small, the inertial term in the Navier−Stokes equations is negligible. The conservation of mass and momentum in the fluid are thus given by

$$\nabla\cdot\mathbf{u} = 0 \qquad \text{in } \Omega \tag{5}$$

and

$$\rho\frac{\partial\mathbf{u}}{\partial t} = -\nabla p + \mu\nabla^2\mathbf{u} \qquad \text{in } \Omega \tag{6}$$

where **u** is the fluid velocity vector, p is the pressure, ρ and μ are, respectively, the fluid density and the dynamic viscosity.

Electro-osmosis induced by solid surface charge is approximated by the Smoluchowski slip velocity on the charged boundary. Hence, the fluid velocity adjacent to the microchannel wall is

$$\mathbf{u} = \frac{\varepsilon_f\zeta_w}{\mu}(\mathbf{I}-\mathbf{nn})\cdot\nabla\phi, \quad \text{on ABCDE and FGHIJ} \tag{7}$$

where ε_f is the permittivity of the fluid, ζ_w is the zeta potential of the channel wall, **I** and **n** are, respectively, the second-order unit tensor and the unit normal vector pointing from the channel wall to the fluid domain. The quantity $(\mathbf{I}-\mathbf{nn})\cdot\nabla\phi$ defines the electric field tangent to the charged channel wall.

The fluid boundary condition on the particle surface includes not only the slip velocity, but also the velocity related to the particle motion, expressed as

$$\mathbf{u} = \mathbf{U_p} + \omega_\mathbf{p}\times(\mathbf{x_s}-\mathbf{x_p}) + \frac{\varepsilon_f\zeta_p}{\mu}(\mathbf{I}-\mathbf{nn})\cdot\nabla\phi \qquad \text{on } \Gamma \tag{8}$$

In the above, the first term, $\mathbf{U_p}$, denotes the translational velocity. The second term denotes the particle rotation, including the angular velocity, $\boldsymbol{\omega_p}$, the position vector of the particle's surface, $\mathbf{x_s}$, and the position vector of the particle's center, $\mathbf{x_p}$. The last term in eq 8 represents the electro-osmotic slip velocity adjacent to the particle with ζ_p denoting the zeta potential of the particle.

The total force exerting on the particle consists of the hydrodynamic force, $\mathbf{F_H}$, arising from the fluid motion outside of the EDL, and the electrokinetic force, $\mathbf{F_E}$, which are obtained, respectively, by integrating the hydrodynamic stress tensor $\mathbf{T^H}$ and the Maxwell stress tensor $\mathbf{T^E}$ over the particle surface

$$\mathbf{F_H} = \int \mathbf{T^H}\cdot\mathbf{n}\,d\Gamma = \int[-p\mathbf{I}+\mu(\nabla\mathbf{u}+\nabla\mathbf{u}^T)]\cdot\mathbf{n}\,d\Gamma \tag{9}$$

and

$$\mathbf{F_E} = \int \mathbf{T^E}\cdot\mathbf{n}\,d\Gamma = \int\left[\varepsilon_f\mathbf{EE}-\frac{1}{2}\varepsilon_f(\mathbf{E}\cdot\mathbf{E})\mathbf{I}\right]\cdot\mathbf{n}\,d\Gamma \tag{10}$$

where **E** is the electric field related to the electric potential by $\mathbf{E} = -\nabla\phi$. Using eq 2, the first term of the integrand in the right-hand side (RHS) of eq 10 vanishes.[41] Therefore, eq 10 represents the pure DEP force acting on the particle. The van der Waals force, which is very small comparing to the hydrodynamic and DEP forces, is neglected in the current study.

(41) Hsu, J.-P.; Yeh, L.-H.; Ku, M.-H. *J. Colloid Interface Sci.* **2007**, *305*, 324.

The translational velocity of the particle is governed by the Newton's second law

$$m_p \frac{d\mathbf{U_p}}{dt} = \mathbf{F_H} + \mathbf{F_E} \quad (11)$$

where m_p is the mass of the particle.

The angular velocity of the particle is determined by

$$I_p \frac{d\omega_p}{dt} = \mathbf{Q} = \int (\mathbf{x_s} - \mathbf{x_p}) \times (\mathbf{T^H} \cdot \mathbf{n})\, d\Gamma + \int (\mathbf{x_s} - \mathbf{x_p}) \times (\mathbf{T^E} \cdot \mathbf{n})\, d\Gamma \quad (12)$$

where I_p is the moment of inertia of the particle and $\mathbf{Q}$ is the torque exerting on the particle. When the DEP effect is not considered, the last terms in the RHS of eqs 11 and 12 are omitted.

The center $\mathbf{x_p}$ and the orientation $\boldsymbol{\theta_p}$ of the particle are expressed by

$$\mathbf{x_p} = \mathbf{x_{p0}} + \int_0^t \mathbf{U_p}\, dt \quad (13)$$

and

$$\theta_p = \theta_{p0} + \int_0^t \omega_p\, dt \quad (14)$$

where $\mathbf{x_{p0}}$ and $\boldsymbol{\theta_{p0}}$ denote, respectively, the initial location and orientation of the particle.

The aforementioned equations are defined in the ALE framework, in which the fluid flow and the electric field are solved in an Eulerian framework, and meanwhile the particle motion is tracked in a Lagrangian manner.[42,43] After each computational time step, the mesh is deformed to adapt the new location and orientation of the particle based on eqs 13 and 14. When the mesh quality degrades to a designated level as the particle translates and rotates, a new geometry with an undeformed mesh is created on the basis of the preceding deformed mesh. Subsequently, the previous solutions of the fluid flow and the electric field in the deformed mesh are projected onto the undeformed mesh to continue the computation until the next mesh regeneration. Therefore, the ALE algorithm can track a long way particle transport, which is of great interest in the present study.

The particle−fluid−electric field coupled system is simultaneously solved with a commercial finite-element package COMSOL (version 3.4a, www.comsol.com) operating in a high-performance cluster. The computational domain Ω in Figure 2 is discretized into quadratic triangular elements with a higher density around the particle. Rigorous mesh-independence tests have been performed to ensure that all solutions obtained are fully converged and independent of grid density. The proposed ALE algorithm has been successfully used to simulate the pressure-driven particle transport through a converging-diverging microchannel, showing a good agreement with experimental results.[44] In addition, the particle trajectory shift in a constricted channel due to the DEP effect, predicted by the present particle-fluid-electric field coupled model, shows quantitative agreement with the experimental observation.[37] The results of experiments and numerical simulations for the electrokinetic particle transport in the L-shaped microchannel are also compared in the following section to validate the present numerical model as well as the developed ALE code.

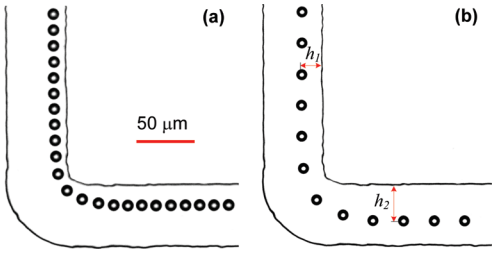

Figure 3. Trajectories of a 10 μm particle moving through the L-shaped channel under an electric field of 6 KV/m (a) and 12 KV/m (b). Time interval between adjacent particles is 0.14 s.

4. Results and Discussion

The average electrokinetic mobilities of 4 and 10 μm particles are, respectively, determined to be 4.0×10^{-8} m^2/(V·s) and 1.6×10^{-8} m^2/(V·s) by measuring the average velocities of the particles in the upstream section where the DEP effect is almost negligible. The following fluid viscosity and permittivity, $\mu = 1.0 \times 10^{-3}$ kg/(m·s) and $\varepsilon_f = 6.9 \times 10^{-10}$ F/m, are used in the numerical study. The particle electrokinetic mobility, η, considering the effect of channel wall is given as[6]

$$\eta = (1 - 0.267699\lambda^3 + 0.338324\lambda^5 - 0.040224\lambda^6) \times \frac{\varepsilon_f}{\mu}(\zeta_p - \zeta_w) \quad (15)$$

where $\lambda = a/d$ with d being the perpendicular distance between the particle's center and the channel wall. On the basis of the reported ζ potential of PDMS, $\zeta_w = -80$ mV,[4,45] the measured particle mobility, values of the fluid viscosity and permittivity, the ζ potentials of the 4 and 10 μm particles were estimated from eq 15 as −56.8 and −22.0 mV, respectively. Without specific statement, the ζ potentials of the two particles in the following numerical simulations are exactly the same as the above two values. The channel width b and channel length L are, respectively, 53 and 200 μm. The radii of arc connections at the inner and outer corners are, respectively, 10 and 63 μm. Although the simulation only covers the L-shaped section of the actual device, the electric potential difference between the inlet and outlet in the numerical study is scaled from the actual value in the experiments to obtain the same electric field. The electric field intensity mentioned below is calculated by dividing the applied electric potential difference over the total length of the centerline of the microchannel.

4.1. Experimental Results. Figure 3 illustrates the trajectory of a 10 μm particle migrating through the L-shaped channel under an electric field of 6 KV/m (a) and 12 KV/m (b). These trajectories are obtained by superposing sequential images of a single particle. The time interval between adjacent images is 0.14 s. From eq 10, it can be seen that the DEP force can be amplified as the particle size and the magnitude of the applied electric field increase. The trajectories of the 4 μm particles (results are not shown here) almost follow the flow streamlines due to a minimal DEP effect, while the 10 μm particle experiences a significant trajectory shift after passing the corner of the L-shaped channel. Figure 1b shows

(42) Hu, H. H.; Joseph, D. D.; Crochet, M. J. *Theor. Comput. Fluid Dyn.* **1992**, *3*, 285.
(43) Hu, H. H.; Patankar, N. A.; Zhu, M. Y. *J. Comput. Phys.* **2001**, *169*, 427.
(44) Ai, Y.; Joo, S. W.; Jiang, Y.; Xuan, X.; Qian, S. *Biomicrofluidics* **2009**, *3*, 022404.
(45) Venditti, R.; Xuan, X. C.; Li, D. Q. *Microfluid. Nanofluid.* **2006**, *2*, 493.

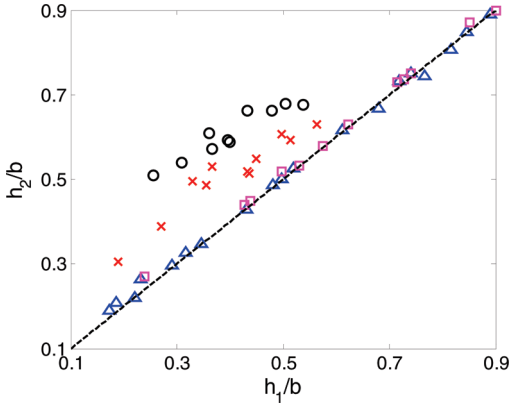

Figure 4. Trajectory shift for particles of different sizes under different electric field intensities. Circles and crosses represent, respectively, the trajectory shifts of 10 μm particles under electric fields of 12 and 6 KV/m. Squares and triangles represent, respectively, the trajectory shifts of 4 μm particles under 12 and 6 KV/m. The dashed line is a reference line corresponding to $h_1 = h_2$.

that the most nonuniform distribution of the electric field occurs at the corner section in the presence of a particle, resulting in a negative DEP force pointing from the higher electric field region at the inner corner to the lower electric field region at the outer corner. The induced DEP force around the corner shifts the particle trajectory from inner streamlines to outer streamlines, which was also observed around the corner in a constricted microchannel[4,8] and used for particle separation and focusing.[5,23−29]

It was observed that all 10 μm particles were moving within the middle $^2/_3$ of the microchannel width region at the upstream; while 4 μm particles could move closer to the channel wall. This is mainly due to the DEP repulsive force arising form the dielectric interaction between the particle and the channel wall. The particle incoming location at the upstream h_1 and outgoing location at the downstream h_2, normalized by the channel width, are summarized in Figure 4 to show the trajectory shift of the 4 and 10 μm particles under the two different electric fields (6 and 12 KV/m). Figure 4 demonstrates that the trajectory shift of the 4 μm particles is insignificant because of an insufficient particle size and thus a low DEP force acting on the particles. The trajectory shift of the 10 μm particles depends on the electric field magnitude since a stronger electric field results in a larger DEP force exerting on the particle, thus inducing a larger trajectory shift.

4.2. Comparison between Experimental and Numerical Results. Figure 5 compares the experimental particle trajectories to numerical predictions obtained by the proposed model as described in section 3. The experimental (symbols) and predicted (lines) trajectories of two 10 μm particles initially located at $h_1/b = 0.27$ (circles, dashed line, and dash−dotted line in Figure 5a) and $h_1/b = 0.47$ (triangles and solid line in Figure 5a) in the upstream under an electric field of 12 KV/m are superposed in Figure 5a. For the particle initially located at $h_1/b = 0.27$ in the upstream, the numerical predictions without (dash-dotted line) and with (dashed line) DEP are in good agreement with the experimental data (circles) in the upstream. However, the prediction without DEP significantly deviates from the experimental data in the corner and the downstream of the microchannel. The prediction with DEP (dashed line in Figure 5a) is in good agreement with the experimental data (circles in Figure 5a), demonstrating that the DEP effect must be taken into account in the study of electrokinetic particle transport in microfluidic channels where spatially nonuniform electric

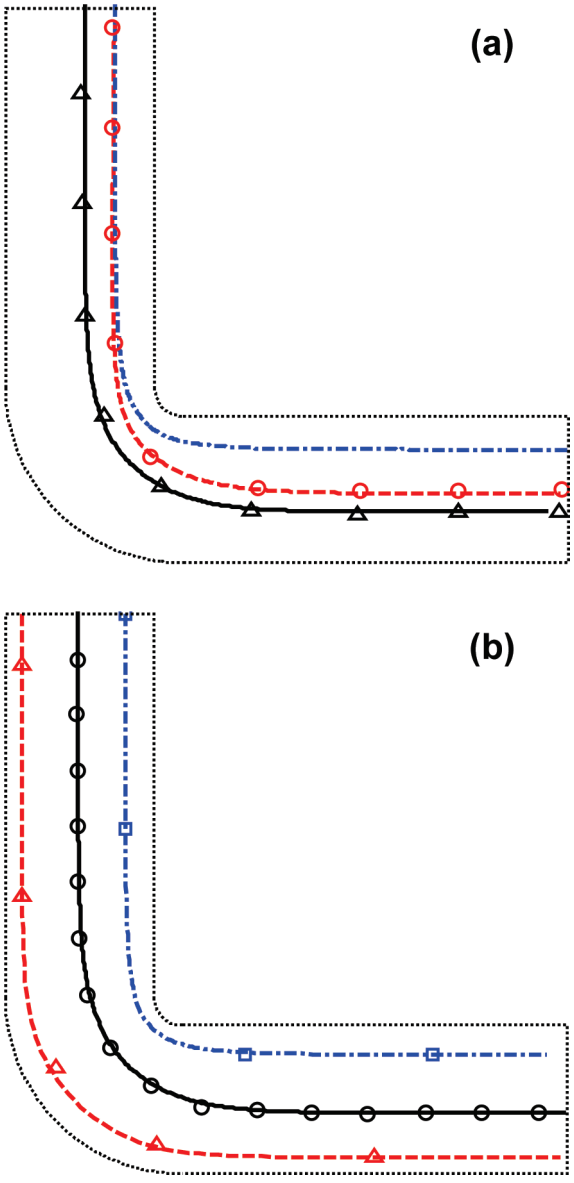

Figure 5. Comparisons between experimental (symbols) and predicted (lines) particle trajectories: (a) 10 μm particles located at $h_1/b = 0.27$ (circles, dashed line, and dash−dotted line) and $h_1/b = 0.47$ (triangles and solid line) under an electric field of 12 KV/m. The dash−dotted line denotes the numerical prediction without DEP; (b) 10 μm particle located at $h_1/b = 0.51$ (circles and solid line) under an electric field of 6 KV/m, and 4 μm particles located at $h_1/b \approx 0.2$ (squares and dash−dotted line) and $h_1/b = 0.89$ (triangles and dashed line) under an electric field of 12 KV/m. The DEP effect is considered in all the numerical predictions.

fields are present; unfortunately, this issue was ignored in most previous studies.[32−35] The good agreement between the predictions with and without DEP in the upstream section of the microchannel demonstrates that the DEP effect is almost negligible in the straight section. The numerical predictions of the 10 μm particle initially located at $h_1/b = 0.47$ under 12 KV/m (solid line in Figure 5a) and at $h_1/b = 0.51$ under 6 KV/m (solid line in Figure 5b) are in good agreement with the corresponding experimental results (triangles in Figure 5a and circles in Figure 5b). Similarly, the numerical predictions of the 4 μm particle initially located at $h_1/b \approx 0.2$ (dash−dotted line in Figure 5b) and at $h_1/b = 0.89$ (dashed line in Figure 5b) under 12 KV/m are in good agreement with the corresponding

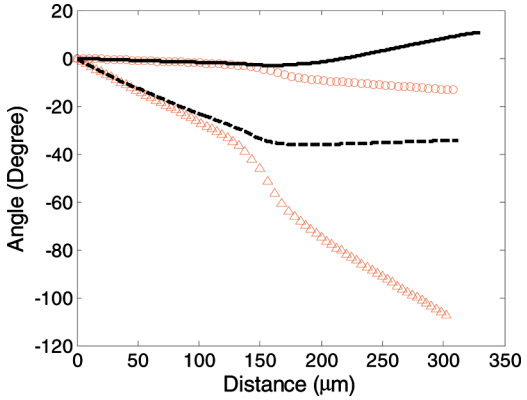

Figure 6. Rotation angles of two 10 μm particles initially located at $h_1/b = 0.27$ (dashed line and triangles) and $h_1/b = 0.47$ (solid line and circles) through the L-shaped channel under an electric field of 12 KV/m. Symbols and lines represent, respectively, numerical predictions without and with DEP.

experimental results (squares and triangles in Figure 5b), demonstrating that the mathematical model capture the physics of the electrokinetic particle transport process. The good agreement between the experimental data and the numerical predictions also confirms the validity of the present numerical model and algorithm adopted here.

4.3. Particle Rotation. Besides the particle trajectory shift, the DEP effect also alters the particle rotation as shown in Figure 6. Solid line and circles represent the predicted angles of the 10 μm particle initially located at $h_1/b = 0.47$ in the upstream from the model with and without DEP, respectively. Dashed line and triangles represent, respectively, the predicted angles of the 10 μm particle initially located at $h_1/b = 0.27$ in the upstream from the model with and without DEP. It is noted that counterclockwise angle is defined as positive hereafter. Because the DEP effect is minimal in the straight section as mentioned above, the particle rotations with (lines) and without (symbols) DEP are almost the same at the upstream. As the particle passes through the corner, the particle angle with considering the DEP effect differs significantly from that without DEP. The particle rotation without DEP shows a similar trend to that reported in a previous study which ignored the DEP effect.[32]

Figure 7 illustrates the rotational dynamics of two 10 μm particles initially located at $h_1/b = 0.12$ (located in the zone A in Figure 7) and $h_1/b = 0.88$ (located in the zone B in Figure 7) along their trajectories through the L-shaped channel under an electric field of 12 KV/m. Since the electric field between the particle and the channel wall is intensified due to the presence of the particle, fluid velocity between the particle and channel wall is higher than that on the other side, inducing a net torque on the particle. Therefore, the angular velocity of particles close to the channel wall is higher than that in the middle channel width region. Furthermore, the rotational direction of particles located in zone A, referring to the inner half channel width region, is clockwise; while the other one located in zone B, outer half channel width region, is counterclockwise. When the electric field distribution around the particle is symmetric, such as the case of particles locating at the centerline of the straight section, the particle rotation cannot occur. However, the particles migrating along the centerline of the corner experience a net torque due to an asymmetric electric field. The particle initially located at $h_1/b = 0.12$ is significantly shifted toward the centerline of the channel downstream. The particle initially located at $h_1/b = 0.88$ displays a slighter trajectory shift after passing the corner, suggesting a less

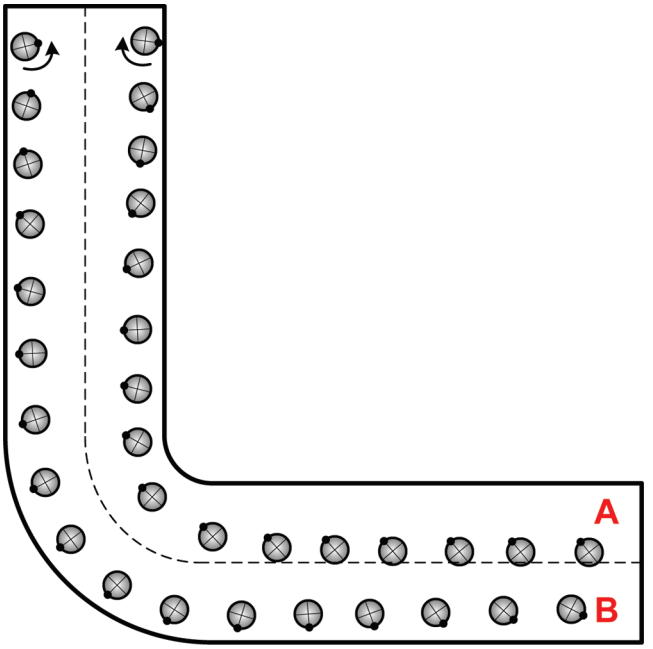

Figure 7. Rotation of two 10 μm particles initially located at $h_1/b = 0.12$ and 0.88 through the L-shaped channel under an electric field of 12 KV/m. The crosses inside the particle and the dot on the particle surface are used for a clear demonstration of the particle's rotation.

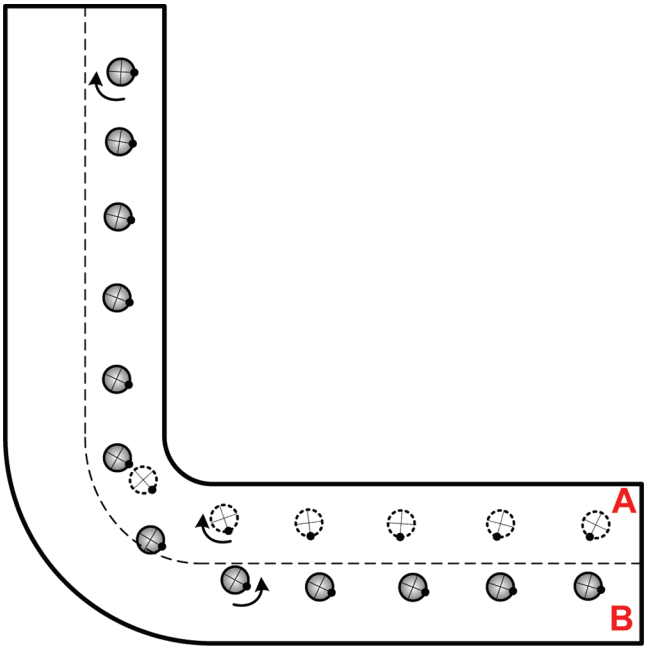

Figure 8. Rotation of a 10 μm particle initially located at $h_1/b = 0.26$ through the L-shaped channel under an electric field of 20 KV/m. The solid and hollow particles represent, respectively, the numerical predictions with and without DEP.

DEP effect at the outer corner. As the particle is less shifted toward the centerline, the angular velocity at the downstream is higher compared to the case of $h_1/b = 0.12$. Therefore, the DEP effect could shift the particle trajectory and also alter the particle's rotational dynamics, which is highly dependent on the particle's location.

Figure 8 shows the rotational dynamics of a 10 μm particle initially located at $h_1/b = 0.26$ through the L-shaped channel

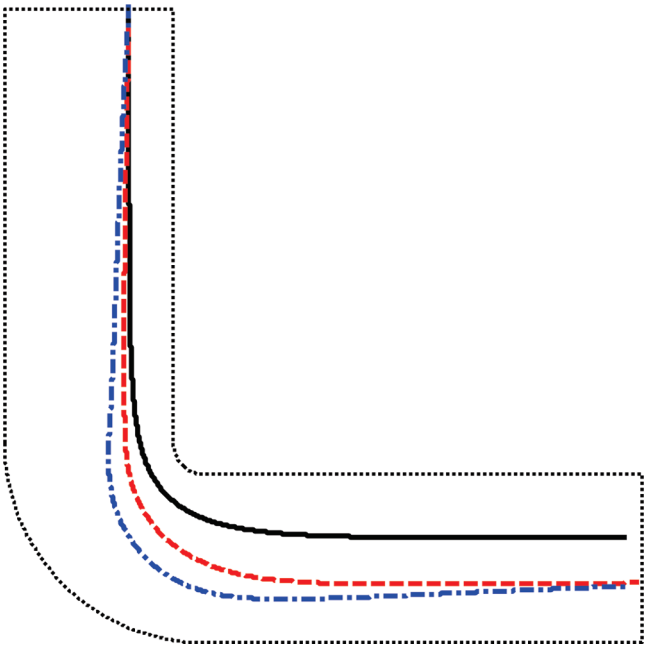

Figure 9. Trajectories of particles of 4 μm (solid line), 10 μm (dashed line) and 15 μm (dash−dotted line) in diameter through the L-shaped microchannel under an electric field of 20 KV/m. The ζ potential of the particle is −56.8 mV and the particle is initially located at $h_1/b = 0.26$ in the upstream.

under an electric field of 20 KV/m. The particle with a solid circle and a hollow circle refer to, respectively, the numerical predictions with and without DEP. As the particle is shifted from zone A to zone B, the rotational direction is altered once it crosses the centerline of the channel. The trajectory and rotation of the particle in the upstream without DEP is quite similar to that with DEP, and thus not displayed in Figure 8. When the DEP effect is ignored, the particle remains in zone A and maintains the same rotational direction after passing through the corner. Thus, the precise estimation of the DEP effect is crucial for the prediction of particle dynamics. It is predicted that the particles initially located in zone A can be shifted to zone B as the electric field further increases (results are not shown here), suggesting that incoming particles with random initial rotational directions can come out with a consistent rotational direction.

4.4. Effect of Particle Size. Trajectories of three particles of different sizes (4, 10, and 15 μm in diameter) initially located at $h_1/b = 0.26$ in the upstream through the L-shaped channel are shown in Figure 9. All of them are bearing an equal ζ potential of −56.8 mV, corresponding to an electrokinetic mobility of 1.6×10^{-8} m^2/(V·s). The 10 μm particle (dashed line) experiences a much larger trajectory shift than the 4 μm particle (solid line), indicating a potential size-based separation in an L-shaped microchannel. Most present DEP separation techniques are based on the same principle that particles in different sizes experience different DEP forces. The 15 μm particle (dash−dotted line) follows a distinct trajectory from that of the 10 μm particle in the corner. However, both particles recover to almost the same location at the outlet due to the repulsive DEP force originated from interactions between the channel wall in the downstream and the particle. Hence, too large particles may not be separated using the current parameters and geometry. But one can still adjust the electric field and geometry (such as channel width and the turn radii) to achieve the separation for specific particle sizes.

4.5. Effect of Electric Field. Besides the particle size, adjusting the electric field is also beneficial to achieve different

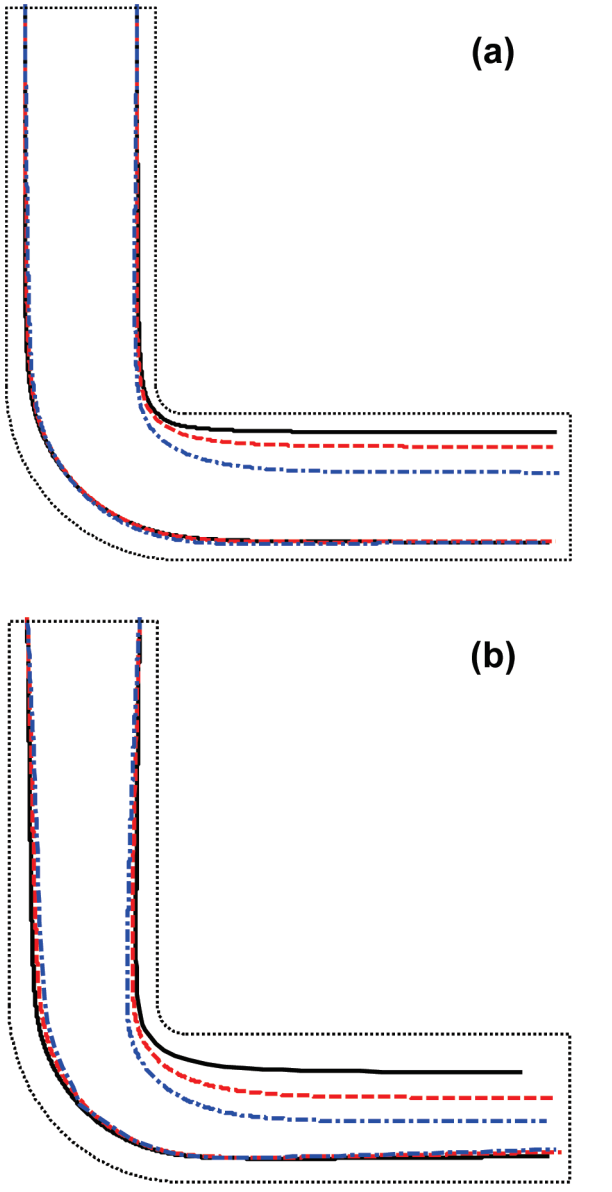

Figure 10. (a) Trajectories of two 4 μm particles initially located at $h_1/b = 0.12$ and 0.88 in the upstream under an electric field of 12 (solid line), 40 (dashed line), and 100 KV/m (dash−dotted line); (b) trajectories of two 10 μm particles initially located at $h_1/b = 0.12$ and 0.88 in the upstream under an electric field of 6 (solid line), 12 (dashed line), and 20 KV/m (dash−dotted line).

trajectory shifts. Figure 10 illustrates the focusing of two 4 μm particles (a) and two 10 μm particles (b) initially located at $h_1/b = 0.12$ and 0.88 in the upstream through the L-shaped channel under different electric fields. The 4 μm particle (Figure 10a) bearing a ζ potential of −22.0 mV, corresponding to the electrokinetic mobility measured in the experiment, shows a negligible focusing under a 12 KV/m (solid lines), and a slight focusing effect under 40 KV/m (dashed lines) and 100 KV/m (dash−dotted lines). The particle focusing ratios w_1/w_2, defined as the particle flow width at the inlet dividing by that at the outlet, are 1.17 and 1.59 corresponding to the electric fields of 40 and 100 KV/m, respectively. In contrast, a distinct focusing effect of the 10 μm particle (Figure 10b) bearing a ζ potential of −56.8 mV is observed as shown in Figure 10b. The particle focusing ratios w_1/w_2 are 1.34, 2.06, and 3.89 corresponding to the electric fields of 6 (solid lines), 12 (dashed lines), and 20 KV/m (dash−dotted

lines), respectively. This kind of particle focusing effect in the case of constricted[28,29] and serpentine channels[31] has also been experimentally observed in previous studies.

5. Conclusions

The effects of the DC DEP force, arising from the interactions between the nonuniform electric field around the corner and the dielectric particle, on the electrokinetic particle transport through an L-shape microchannel, are experimentally and numerically studied. The good agreement between experimental results and numerical predictions verifies that the proposed multiphysics model is able to predict the electrokinetic transport of particles in complex microfluidic channels. Comparisons between numerical predictions without and with DEP and the obtained experimental results prove that the DEP effect must be taken into account in the study of electrokinetic particle transport in nonuniform electric fields. Results indicate that the DEP-induced particle trajectory shift in the L-shaped microchannel depends on the electric field and particle size. The latter dependence implies a potential DEP separation of particles by size. Numerical studies also demonstrate a strong influence of DEP on the velocity and direction of the particle's rotations.

Acknowledgment. This work is supported by the World Class University Grant No. R32-2008-000-20082-0 of the Ministry of Education, Science and Technology of Korea (SQ), and NSF Grant CBET-0853873 with Marc S. Ingber as the grant monitor (XX).